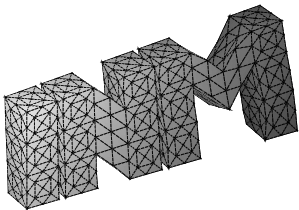


---

A Fast BE-FE Coupling Scheme  
for Partly Immersed Bodies

D. Brunner, G. Of, M. Junge, O. Steinbach, L. Gaul

---



**Berichte aus dem  
Institut für Numerische Mathematik**



**Technische Universität Graz**

---

**A Fast BE-FE Coupling Scheme  
for Partly Immersed Bodies**

D. Brunner, G. Of, M. Junge, O. Steinbach, L. Gaul

---

**Berichte aus dem  
Institut für Numerische Mathematik**

Bericht 2008/5

Technische Universität Graz  
Institut für Numerische Mathematik  
Steyrergasse 30  
A 8010 Graz

**WWW:** <http://www.numerik.math.tu-graz.at>

© Alle Rechte vorbehalten. Nachdruck nur mit Genehmigung des Autors.

# A Fast BE-FE Coupling Scheme for Partly Immersed Bodies

Dominik Brunner<sup>1</sup>, Günther Of<sup>2</sup>, Michael Junge<sup>1</sup>, Olaf Steinbach<sup>2</sup>  
and Lothar Gaul<sup>1</sup>

<sup>1</sup>Institute of Applied and Experimental Mechanics, University of Stuttgart,  
Pfaffenwaldring 9, 70550 Stuttgart, Germany

<sup>2</sup>Institute of Computational Mathematics, Graz University of Technology,  
Steyrergasse 30/III, 8010 Graz, Austria

## Abstract

Fluid-structure coupled problems are investigated to predict the vibro-acoustic behavior of submerged bodies. The finite element method is applied for the structural part, whereas the boundary element method is used for the fluid domain. The focus of this paper is on partly immersed bodies. The fluid problem is favorably modeled by a half-space formulation. This way, the Dirichlet boundary condition on the free fluid surface is incorporated by a half-space fundamental solution. A fast multipole implementation is presented for the half-space problem. In case of a high density of the fluid, the forces due to the acoustic pressure which act on the structure can not be neglected. Thus, a strong coupling scheme is applied. An iterative solver is used to handle the coupled system. The efficiency of the proposed approach is discussed using a realistic model problem.

## 1 Introduction

In recent years, the acoustic properties have become a major purchasing criteria for many products. Therefore, special attention is paid to the simulation of the sound radiation of vibrating structures. Basic concepts of acoustics are introduced in [1, 2, 3]. Typically, analytic solutions can only be derived for relative simple structures. More complex structures are treated by discretization methods like the finite element method (FEM) [4] and the boundary element method (BEM) [5], which only discretizes the boundary of the acoustic domain. The application of the BEM to the Helmholtz equation in acoustics is discussed in [6, 7, 8]. A more engineering oriented discussion is given in [9]. For exterior acoustic problems, the main advantage of the BEM compared to the FEM is, that the Sommerfeld radiation condition is implicitly fulfilled by the applied fundamental solution. However, non-uniqueness problems may occur due to spurious modes. Several formulations

are known to overcome this phenomenon. Besides the CHIEF method [10] the Burton–Miller formulation [11, 12] is widely applied. Recently, stabilized BE methods have been presented for Lipschitz boundaries in [13, 14]. The CHIEF method introduces some additional points in the interior domain, whereas the others use a linear combination of two boundary integral equations. The Burton–Miller approach is applied in this paper.

The BEM reduces the problem to a formulation on the boundary and hence the number  $N$  of degrees of freedom. However, the standard BEM leads to fully populated matrices, which is a major drawback compared to sparse matrices resulting from FE discretizations. If additionally a direct solver is applied to solve the BE system, an unfavorable expense in the order of  $\mathcal{O}(N^3)$  results. Iterative methods like a GMRES [15] in combination with suitable preconditioners help to improve this to  $\mathcal{O}(N^2)$ . The application of iterative methods to BEM matrices in acoustics is discussed in [16], which deals with scattering at a rigid cylinder.

The use of the fast multipole method (FMM) reduces the memory requirements and computation times of the matrix-vector product to almost linear complexity. The FMM was first introduced for integral equations of potential theory [17]. The basic idea is to use a series expansion of the kernel to separate the variables and to use a hierarchical clustering to compute the coefficients of the expansion efficiently. A diagonal form of the multipole expansion is discussed in [18, 19, 20]. Here, the convolutions for the translation operators are transferred to a simple multiplication by transformation into the Fourier space. The resulting overall expense using a multilevel scheme is now  $\mathcal{O}(N \log^2 N)$  [21]. A survey of the FMM for the Helmholtz equation is given by [22, 23]. In various papers, the FMM is applied to acoustic problems. An interior acoustic tube is examined in [24], while scattering problems are investigated in [25] and for multiple objects in [26]. The latter one also treats the sound radiation of an engine. Application of the FMM in combination with multifield problems is discussed in [27]. Besides the FMM, Adaptive Cross Approximations and  $\mathcal{H}$ -matrices [28, 7, 29] are used to improve the efficiency of the BEM. A comparison of fast methods is presented in [30, 31].

Besides full-space problems, where a radiating structure is within an infinite acoustic domain, also problems with a given boundary condition on an infinite plane are of interest. These problems can efficiently be simulated using a half-space fundamental solution [32, 33, 34].

In this paper, fluid-structure coupled problems are investigated. An introduction to this topic is for instance given in [35]. Besides FE-FE coupled problems [4], FE-BE coupling schemes are used for exterior problems [36, 37]. A preconditioning strategy for the iterative solution of the coupled system is proposed by [38]. Also non-conforming coupling schemes with Lagrange multipliers exist for fluid-structure coupled problems [27], where the BE mesh is set up completely independent of the FE mesh. A comparison of the last mentioned methods including different preconditioners is given in [39].

Besides full-space problems, where a radiating structure is within an infinite acoustic domain, also problems with a given boundary condition on an infinite plane are of interest. Such problems arise naturally when computing the radiation of sound from ships. Half-space problems can efficiently be simulated using a half-space fundamental solution [32,

33, 34]. Application of these techniques to a ship model is reported in [40, 41].

In this paper, the fast multipole method is applied to the BEM of the half-space problem. A strong coupling scheme between the FEM for the structural part and the BEM for the exterior fluid domain is presented. In Section 2, the governing equations of the underlying problem are discussed in the frequency domain. In Section 3, the application of the BEM to the half-space problem and its implementation using the FMM is shown. Furthermore, the FE representation of the structural domain and the fully coupled approach are outlined in Sections 4 and 5, respectively. The accuracy and efficiency of the half-space FMM approach is discussed by means of a realistic model problem in Section 6.

## 2 Governing Equations of the Coupled Problem

In the following, the governing equations for the fluid-structure interaction problem are presented. All variables are transformed to the frequency domain with the time harmonic behavior  $e^{-i\omega t}$ , where  $\omega = 2\pi f$  denotes the angular frequency and  $i$  is the imaginary unit. The structural domain  $\Omega_s$  (cf. Figure 1 left) is assumed to be linear elastic with the Lamé constants  $\lambda$  and  $\mu$ . The material is homogeneous with the structural density  $\varrho_s$ . The corresponding elastodynamic problem for the displacements  $u$  is given by

$$\omega^2 \varrho_s u(x) + \mu \Delta u(x) + (\lambda + \mu) \text{grad div } u(x) = 0 \quad \text{for } x \in \Omega_s \subset \mathbb{R}^3, \quad (1)$$

$$T u(x) = t_s(x) \quad \text{for } x \in \Gamma_s, \quad (2)$$

and additionally the transmission condition introduced by (6) and where  $\Gamma_s$  is the surface of the structure which is not in contact with the fluid, see Figure 1, left.

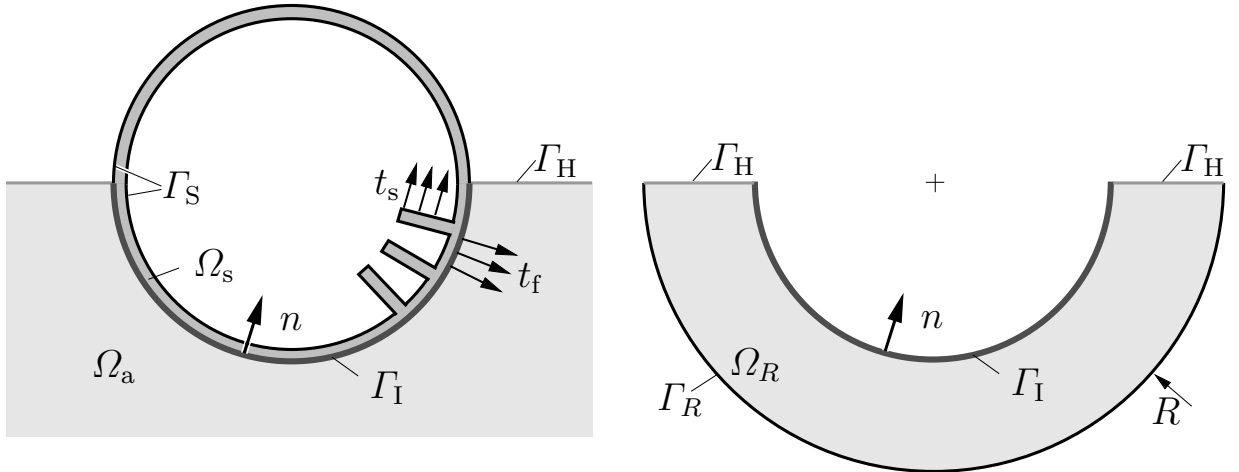


Figure 1: Domains and boundaries of the coupled problem (left) and auxiliary problem of the fluid domain for the derivation of the representation formula (right).

The Laplacian is denoted by  $\Delta$  and  $T$  represents the traction operator. The structure is excited by the prescribed tractions  $t_s$ . The time harmonic Helmholtz equation is applied to

describe the acoustic pressure  $p$  in the fluid domain  $\Omega_a$ . Since a partly immersed structure is investigated in this paper, the free fluid surface  $\Gamma_H$  also has to be modeled by a Dirichlet boundary condition. The acoustic boundary value problem reads

$$\Delta p(x) + \kappa^2 p(x) = 0 \quad \text{for } x \in \Omega_a, \quad (3)$$

$$p(x) = 0 \quad \text{for } x \in \Gamma_H, \quad (4)$$

$$\left| \frac{\partial p}{\partial R} - i \kappa p \right| < \frac{c_f}{R^2} \quad \text{for } R = |x| \rightarrow \infty, \quad (5)$$

where the additional transmission condition is given by (7). The circular wave number is denoted by  $\kappa = \frac{\omega}{c_f}$  and the speed of sound is  $c_f$ . Equation (5) is called Sommerfeld radiation condition, which ensures an outgoing wave within the exterior acoustic domain [5]. Since a fluid with a high density is used in the following, the tractions  $t_f$  due to the acoustic pressure are not negligible. Therefore, a strong coupling scheme has to be applied, which is represented by the two transmission conditions

$$T u(x) = t_f(x) = -p(x) n_x \quad \text{for } x \in \Gamma_1, \quad (6)$$

$$q(x) := \frac{\partial p(x)}{\partial n_x} = \omega^2 \varrho_f u(x) n_x \quad \text{for } x \in \Gamma_1, \quad (7)$$

where the acoustic flux  $q$  is introduced. In the next two sections, the application of the BEM for the acoustic boundary value problem and a FEM discretization for the elastodynamic problem is outlined.

### 3 Fluid Domain: Boundary Element Method

To derive a boundary integral representation of the pressure solution of the acoustic problem, an auxiliary domain  $\Omega_R$  as depicted in Figure 1 (right) is introduced which reaches  $\Omega_a$  in the limit case  $R \rightarrow \infty$ . The closed boundary of  $\Omega_R$  is split into the three parts  $\bar{\Gamma}_1 \cup \bar{\Gamma}_H \cup \bar{\Gamma}_R = \Gamma$ . Starting point is Green's second identity

$$\int_{\Omega_R} \Delta p(y) g(y) dy = \int_{\Omega_R} \Delta g(y) p(y) dy + \int_{\Gamma} g(y) \frac{\partial p(y)}{\partial n_y} ds_y - \int_{\Gamma} p(y) \frac{\partial g(y)}{\partial n_y} ds_y \quad (8)$$

for the closed domain  $\Omega_R$  with the exterior normal  $n_y$ . Plugging (3) into (8) yields

$$\int_{\Omega_R} (\Delta g(y) + \kappa^2 g(y)) p(y) dy + \int_{\Gamma} g(y) \frac{\partial p(y)}{\partial n_y} ds_y - \int_{\Gamma} \frac{\partial g(y)}{\partial n_y} p(y) ds_y = 0.$$

Choosing the function  $g(y)$  as the fundamental solution  $P^*(x, y)$  of the Helmholtz equation, leads to the representation formula

$$p(x) = \int_{\Gamma} P^*(x, y) \frac{\partial p(y)}{\partial n_y} ds_y - \int_{\Gamma} \frac{\partial P^*(x, y)}{\partial n_y} p(y) ds_y \quad \text{for } x \in \Omega_R. \quad (9)$$



For the investigated half-space problem, the modified fundamental solution [32, 33, 34]

$$P^*(x, y) = \frac{1}{4\pi} \frac{e^{i\kappa|x-y|}}{|x-y|} + R_H \frac{1}{4\pi} \frac{e^{i\kappa|\tilde{x}-y|}}{|\tilde{x}-y|}, \quad (10)$$

is advantageous. For a pressure-free water surface, a reflexion coefficient  $R_H = -1$  has to be chosen. For simplicity it is assumed that the half-space boundary  $\Gamma_H$  is located at  $x_3 = 0$ . Thus,  $\tilde{x} = (x_1, x_2, -x_3)$  denotes a point which is mirrored at the plane  $x_3 = 0$ . To derive a simpler version of the representation formula, the integrals in (9) over the three boundaries  $\Gamma_I$ ,  $\Gamma_H$  and  $\Gamma_R$  are investigated in detail.

Using the Sommerfeld radiation condition (5) in the usual way, one can show, that

$$\int_{\Gamma_R} P^*(x, y) \frac{\partial p(y)}{\partial n_y} ds_y - \int_{\Gamma_R} \frac{\partial P^*(x, y)}{\partial n_y} p(y) ds_y \rightarrow 0 \quad \text{as } R \rightarrow \infty$$

and thus these integrals vanish in the limit process  $R \rightarrow \infty$ . A closer look to the integrals over the half-space surface reveals

$$\int_{\Gamma_H} P^*(x, y) \frac{\partial p(y)}{\partial n_y} ds_y - \int_{\Gamma_H} \frac{\partial P^*(x, y)}{\partial n_y} p(y) ds_y = 0.$$

The first integral vanishes, since the modified fundamental solution (10) is zero for  $y \in \Gamma_H$ . The second one cancels out because of the zero pressure boundary condition on  $\Gamma_H$ . This way, one obtains a simplified version of the representation formula (9)

$$p(x) = \int_{\Gamma_I} P^*(x, y) \frac{\partial p(y)}{\partial n_y} ds_y - \int_{\Gamma_I} \frac{\partial P^*(x, y)}{\partial n_y} p(y) ds_y, \quad x \in \Omega_a. \quad (11)$$

Advantages of the half-space approach are, that the zero pressure boundary condition is exactly fulfilled and the water surface does not have to be meshed at all which reduces the number of degrees of freedom. The representation formula (9) is valid for a point  $x$  within the acoustic domain  $\Omega_a$ .

The limit process  $x \rightarrow \Gamma_I$  yields the boundary integral equations

$$\frac{1}{2}p(x) = \underbrace{\int_{\Gamma_I} P^*(x, y) \frac{\partial p(y)}{\partial n_y} ds_y}_{=: (Vq)(x)} - \underbrace{\int_{\Gamma_I} \frac{\partial P^*(x, y)}{\partial n_y} p(y) ds_y}_{=: (Kp)(x)}, \quad x \in \Gamma_I, \quad (12)$$

$$\frac{1}{2}q(x) = \underbrace{\int_{\Gamma_I} \frac{\partial P^*(x, y)}{\partial n_x} \frac{\partial p(y)}{\partial n_y} ds_y}_{=: (K'q)(x)} - \underbrace{\frac{\partial}{\partial n_x} \int_{\Gamma_I} \frac{\partial P^*(x, y)}{\partial n_y} p(y) ds_y}_{=: -(Dp)(x)}, \quad x \in \Gamma_I, \quad (13)$$

for a smooth boundary with the single layer potential  $V$ , the double layer potential  $K$ , its adjoint  $K'$  and the hypersingular operator  $D$ . If the point  $x$  is on the half-space plane  $x_3 = 0$ , the coefficient of the integral-free term changes due to an extra jump relation [33, 34]. In the following, a Galerkin variational formulation is used for which this

extended jump relation is not needed, if the integration points are not located on the half-space plane.

It is well known, that neither the boundary integral equation (12) nor the hypersingular boundary integral equation (13) has an unique solution for all frequencies. Therefore, the so-called Burton–Miller approach [12] is applied to overcome the non-uniqueness problem. This method uses a linear combination of the boundary integral equations (12) and (13) with a scalar coefficient  $\alpha = -i/\kappa$ . The Galerkin formulation reads

$$\begin{aligned} & \int_{\Gamma_1} \nu(x) \left( \frac{1}{2}I + K \right) p(x) ds_x - \alpha \int_{\Gamma_1} \nu(x) (Dp)(x) ds_x \\ &= \int_{\Gamma_1} \nu(x) (Vq)(x) ds_x + \alpha \int_{\Gamma_1} \nu(x) \left( -\frac{1}{2}I + K' \right) q(x) ds_x \end{aligned} \quad (14)$$

with a weighting function  $\nu(x)$ . The boundary is discretized with plane triangular elements. Piecewise linear and continuous basis functions  $\varphi_i(x)$  are used for the approximation of  $p$  and  $\nu$  and piecewise constant ones for  $q$ . The resulting system of linear equations reads

$$\underbrace{\left( \frac{1}{2}M + K - \alpha D \right)}_{=: \mathbf{K}_{BE}} \mathbf{p} - \underbrace{\left( \mathbf{V} - \frac{1}{2}\alpha \mathbf{M}' + \alpha \mathbf{K}' \right)}_{=: \mathbf{C}_{BE}} \mathbf{q} = 0, \quad (15)$$

with the nodal pressure vector  $\mathbf{p}$  and the element flux vector  $\mathbf{q}$ .

### 3.1 Standard Implementation of the Half-Space Problem

For the implementation of the modified fundamental solution, a strategy is chosen, which is later transferred to the multipole algorithm and turns out to be quite simple and efficient. As point  $\tilde{x}$  in (10) is mirrored at the half-space plane, the whole model is mirrored (cf. Figure 2) for the realization. This mirror technique is also called method of images or reflexion principle. In the following, the evaluation of the matrix-vector product  $\mathbf{w} = \mathbf{V}\mathbf{q}$  is considered for the Galerkin matrix of the single-layer potential with piecewise linear test functions and constant trial functions with a vector  $\mathbf{q}$

$$w_m = \sum_{k=1}^{N_e} V[m, k] q_k \quad \text{for } m = 1, \dots, N_I. \quad (16)$$

The matrix entries are computed by

$$\begin{aligned} V[m, k] &= \int_{\Gamma} \int_{\tau_k} \nu_m(x) P^*(x, y) ds_y ds_x \\ &= \int_{\Gamma_1} \int_{\tau_k} \nu_m(x) P(x, y) ds_y ds_x - \int_{\tilde{\Gamma}_1} \int_{\tau_k} \nu_{m+N_I}(x) P(x, y) ds_y ds_x, \end{aligned} \quad (17)$$

where

$$P(x, y) = \frac{e^{i\kappa|x-y|}}{4\pi|x-y|}$$

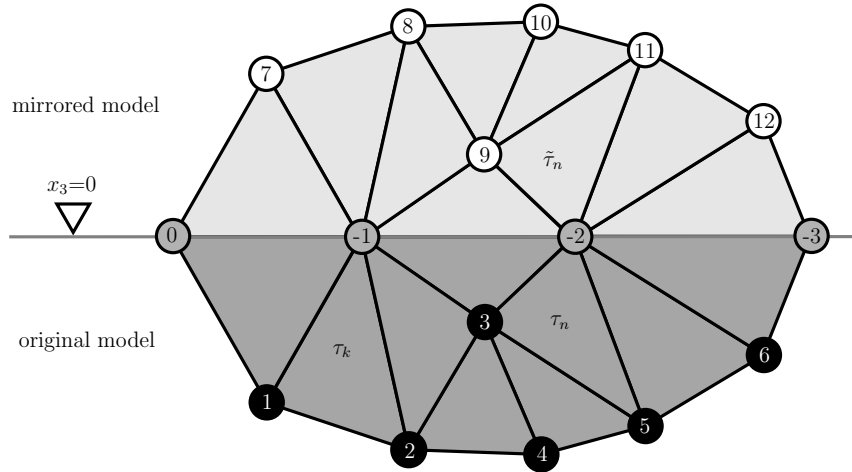


Figure 2: Mirror technique and node order for the implementation of the half-space problem. Only the BE-elements on  $\Gamma_I$  are mirrored.

is the standard fundamental solution, and  $\tilde{\Gamma}_I$  is the mirror image of  $\Gamma_I$ . In the computation of a matrix entry, the integration routines are not only called for the interaction of an element  $\tau_k$  with an original element  $\tau_n$  but also for the interaction with the mirrored element  $\tilde{\tau}_n$ , see Fig. 2. Therefore, the identical set of integration routines are applied for both cases. Please note, that element  $\tau_k$  is always one of the  $N_e$  non-mirrored elements of the model. Finally, the result of the second call, being computed for the mirrored elements, has to be subtracted from the corresponding non-mirrored entries. This is an easy task, if a special node ordering is employed, as visualized in Figure 2. As a Dirichlet boundary condition is specified for the  $N_H$  nodes on the half-space plane  $x_3=0$ , these pressure degrees of freedom drop out during the setup of the Galerkin matrix. Therefore, negative or zero node-identifiers are assigned to them (cf. gray nodes in Fig 2). Consequently, the  $N_I$  non-half-space nodes of the original model start with node-id 1 (black nodes). The node-ids of the mirrored-nodes (white colored) simply result from the corresponding non-mirrored node-ids by addition of  $N_I$ .

The memory consumption for  $\mathbf{K}_{\mathbf{BE}} = [\cdot]_{N_I \times N_I}$  and  $\mathbf{C}_{\mathbf{BE}} = [\cdot]_{N_I \times N_e}$  of (15) is not altered by the mirror-technique. Slightly more memory is needed to store the additional model data with the mirrored elements and nodes.

Due to the realization of the half-space fundamental solution (10) by an additional integration, the computation time is slowed up by a factor  $f$  with respect to the non-mirrored model (here physically not meaningful), with  $1 < f < 2$ . It is less than 2, since the second integration does not have to deal with singular kernels occurring for identical elements.

For standard boundary element methods, the Galerkin matrices  $\mathbf{K}_{\mathbf{BE}}$  and  $\mathbf{C}_{\mathbf{BE}}$  are fully populated resulting in memory requirements and computational efforts of order  $\mathcal{O}(N^2)$  for a problem with  $N$  unknowns. To overcome this drawback, the FMM is applied, resulting in an almost linear expense of order  $\mathcal{O}(N \log^2 N)$ . Especially, in the case of the FMM, the

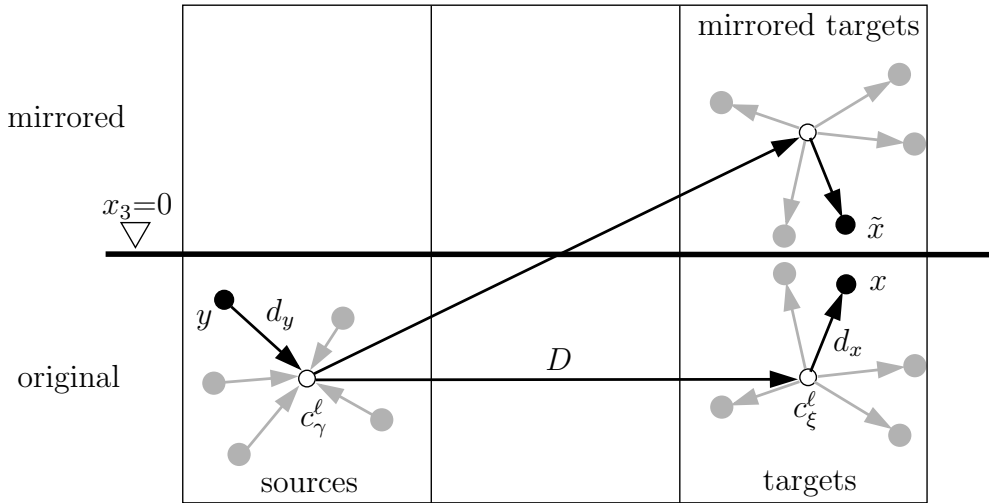


Figure 3: Clustering of the sources and the targets. The vector between  $y$  and  $x$  is split up into the three parts  $d_y$ ,  $D$  and  $d_x$ . The source clusters are only located in the non-mirrored part below the half-space plane  $x_3=0$ .

mirror-technique turns out to be advantageous.

### 3.2 Fast Multilevel Multipole Algorithm for the Half-Space Problem

In this section, the application of the fast multipole method to half-space problems is described. Due to the mirror-technique, the original standard version for the Helmholtz kernel is applied. To avoid convolutions appearing for the standard translation operators, a diagonal form which works in the Fourier space is used [18, 19, 20]. The main concept is based on two ideas, an geometric hierarchy and an approximate expansion of the kernel. Here, the geometric hierarchy is built on the modified model including the mirrored elements. It starts with a box, containing all the elements. The set of the corresponding indices is the so-called root cluster  $C_1^0$ . The clusters  $C_\gamma^{\ell+1}$  on the next finer level  $\ell + 1$  are built by bisection of the corresponding box where the boundary elements  $\tau_k$  are assigned to the clusters  $C_\gamma^{\ell+1}$  with respect to their geometric center point. The geometric center point of a cluster  $C_\gamma^\ell$  is denoted by  $c_\gamma^\ell$ . It is advantageous to have only non-mirrored or mirrored elements in a single cluster, thus the root cluster is always split along the half-space plane. All other clusters are then split along their dominant dimensions. The clusters  $C_\gamma^{\ell+1}$  are called the sons of the father cluster  $C_\xi^\ell$ . The bisection process is repeated recursively until a minimal number of elements within a cluster is reached. Clusters which are not split any more are called leaf-clusters and are denoted by  $\bar{C}_\gamma^\ell$ .

Since the mirror-technique is used here, only the standard Helmholtz kernel has to be

approximated. Starting point is the expansion of the fundamental solution in the form

$$\frac{e^{i\kappa|x-y|}}{4\pi|x-y|} = \frac{i\kappa}{(4\pi)^2} \int_{\mathbb{S}^2} e^{i\kappa d_x \cdot s} M_L(c_\gamma^\ell, c_\xi^\ell, s) e^{i\kappa d_y \cdot s} d\omega_s \quad (18)$$

where  $d_x$  and  $d_y$  are depicted in Figure 3. The so-called translation operator  $M_L$  is defined by [20]

$$M_L(c_\gamma^\ell, c_\xi^\ell, s) := \sum_{\ell=0}^L (2\ell+1) i^\ell h_\ell^{(1)}(\kappa|D|) P_\ell(s \cdot \hat{D}), \quad (19)$$

where  $D = c_\xi^\ell - c_\gamma^\ell$  and  $\hat{D} = D/\|D\|_2$  is the unit direction (cf. Fig 3). In the numerical implementation,  $s$  is represented on a finite set of points on the unit sphere  $\mathbb{S}^2$ . The parameter  $L$  is called expansion length and directly influences the accuracy of the expansion. The semi-empirical rule [42]

$$L(\kappa, d_{\max}) = \kappa d_{\max}^\ell + c_e \log(\kappa d_{\max}^\ell + \pi) \quad (20)$$

is applied, where  $d_{\max}^\ell$  denotes the maximum cluster diameter on level  $\ell$ , and  $c_e$  is a constant which has to be chosen by the user. Since a regular cluster tree is used, the translation operators can be reused.

Since this expansion is only valid for well separated points, one has to distinguish between a far-field (FF), where the expansion is admissible and a near-field (NF), which has to be treated in the classical way. A cluster  $C_\gamma^\ell$  is in the near-field of the cluster  $C_\xi^\ell$  on the same level  $\ell$ , if the condition

$$|c_\gamma^\ell - c_\xi^\ell| \leq c_d \max\{r_\gamma^\ell, r_\xi^\ell\} \quad (21)$$

is fulfilled. Here,  $r_\gamma^\ell$  denotes the radius of the cluster  $C_\gamma^\ell$  and  $c_d$  is a constant which has to be chosen larger than 2. Clusters, whose father clusters satisfy the near-field condition (21), but themselves are not their mutual near-fields, form the interaction list (IL).

The approximate matrix-vector product of (16) with the multilevel FMM is now presented exemplarily for the single layer potential with piecewise linear test functions and constant shape functions. The overall product reads

$$\begin{aligned} w_m &\approx \sum_{k \in \text{NF}(m)} \tilde{V}[m, k] q_k + \frac{i\kappa}{(4\pi)^2} \sum_{\xi | m \in \bar{C}_\xi^\ell} \int_{\Gamma_\xi} \nu_m(x) \int_{\mathbb{S}^2} R(c_\xi^\ell, x, s) N_\xi^\ell(s) d\omega_s ds_x \\ &- \frac{i\kappa}{(4\pi)^2} \sum_{\xi | (m+N_I) \in \bar{C}_\xi^\ell} \int_{\Gamma_\xi} \nu_{m+N_I}(x) \int_{\mathbb{S}^2} R(c_\xi^\ell, x, s) N_\xi^\ell(s) d\omega_s ds_x \end{aligned} \quad (22)$$

where

$$\tilde{V}[m, k] = \int_{\Gamma_I} \int_{\tau_k} \nu_m(x) P(x, y) ds_y ds_x - \delta(m, k) \int_{\tilde{\Gamma}_I} \int_{\tau_k} \nu_{m+N_I}(x) P(x, y) ds_y ds_x \quad (23)$$

with

$$\delta(m, k) = \begin{cases} 1 & \text{for all } k \in \text{NF}(m + N_I) \\ 0 & \text{else.} \end{cases} \quad (24)$$

Note, that  $\xi|m \in \bar{C}_\xi^\ell$  denotes all indices  $\xi$  of leaf clusters  $\bar{C}_\xi^\ell$ , which contain elements which share the node  $m$ . Additionally, the relation

$$R(a, b, s) = e^{i\kappa(b-a) \cdot s} \quad (25)$$

holds. The so-called near-field signatures  $N_\xi^\ell(s)$  are computed by a fast multipole cycle in the following way: First, the far-field signatures  $F_\gamma^\ell(s)$  are computed for all non-mirrored leaf clusters  $\bar{C}_\gamma^\ell$

$$F_\gamma^\ell(s) = \sum_{k \in \bar{C}_\gamma^\ell} \int_{\tau_k} R(y, c_\gamma^\ell, s) q_k \, ds_y. \quad (26)$$

After this, the far-field signatures are converted and summed up as near-field signature for all clusters in the interaction list (IL) (outer-inner translation)

$$N_\xi^\ell(s) = \sum_{C_\gamma^\ell \in \text{IL}(C_\xi^\ell)} M_L(c_\gamma^\ell, c_\xi^\ell, s) F_\gamma^\ell(s), \quad (27)$$

where  $M(c_\gamma^\ell, c_\xi^\ell, s)$  is the translation operator (19). Then, for both sons,  $F_\gamma^\ell(s)$  is shifted to their common father  $C_\zeta^{\ell-1}$  by (outer-outer translation)

$$F_\zeta^{\ell-1}(s) = \sum_{C_\gamma^\ell \in \text{sons}(C_\zeta^{\ell-1})} R(c_\gamma^\ell, c_\zeta^{\ell-1}, s) F_\gamma^\ell \quad (28)$$

and summed up there. The last two steps are repeated until the coarsest level is reached. This completes the upward pass. In the downward pass,  $N_\zeta^\ell(s)$  is shifted to the sons and summed up there by (inner-inner translation)

$$N_\xi^{\ell+1}(s) = N_\xi^{\ell+1}(s) + R(c_\zeta^\ell, c_\xi^{\ell+1}, s) N_\zeta^\ell(s) \quad (29)$$

The last step is repeated until a leaf cluster is reached. There, the solution is recovered by the integration over the unit sphere and the elements, see (22).

The presented FMM algorithm with the mirror-technique has clearly two advantages. First, only a small amount of clusters in the mirrored part are in the near-field of a non-mirrored cluster. Thus, there is only a small number of additional integrations for the sparse near-field matrix. Therefore, the computational time is only slightly increased with respect to a non-mirrored model. As before, the memory consumption for the near-field matrix remains unchanged. The second advantage lies in the multipole compression. Since most of the mirrored clusters are far away from the non-mirrored ones, the interaction is represented on a coarse level, leading to a quite efficient algorithm.

## 4 Structural Domain: Finite Element Method

The discretization of the structural problem (1) and (2) results in a system of linear equations

$$\underbrace{(-\omega^2 \mathbf{M}_s - i\omega \mathbf{D}_s + \mathbf{K}_s)}_{=:\mathbf{K}_{\text{FE}}} \mathbf{u} = \mathbf{f}_s + \mathbf{f}_f, \quad (30)$$

where  $\mathbf{M}_s$  and  $\mathbf{K}_s$  denote the mass matrix and the stiffness matrix, respectively. In this paper, Rayleigh damping is considered with the damping matrix [43]

$$\mathbf{D}_s = \alpha_D \mathbf{M}_s + \beta_D \mathbf{K}_s, \quad (31)$$

and the damping parameters  $\alpha_D$  and  $\beta_D$ . The vector  $\mathbf{f}_s$  incorporates the tractions  $t_s$  due to the driving forces, while the vector  $\mathbf{f}_f$  results from the tractions  $t_f$  on the coupling interface  $\Gamma_1$  and is discussed in the next section, which focuses on the formulation of the coupled problem.

The finite element package ANSYS is utilized to set up the matrices  $\mathbf{M}_s$ ,  $\mathbf{K}_s$  and the right hand side vector  $\mathbf{f}_s$ . They are imported into the research code by a binary interface [44]. This data exchange only has to be done once for a given model, as  $\mathbf{M}_s$  and  $\mathbf{K}_s$  are frequency independent. Typically, shell elements with rotational degrees of freedom are applied for thin structures. Thus, each node has six degrees of freedom, which are  $\{u_x, u_y, u_z, \theta_x, \theta_y, \theta_z\}$ .

## 5 Coupled Problem

In this section, the discrete coupled system is formulated using the BE system (15), the FE system (30) and the transmission conditions. Here, matching grids for the FE and the BE part are considered. The first transmission condition (6) links the acoustic pressure  $p$  with the tractions  $t_f$  of the structure and reads in matrix notation

$$\mathbf{f}_f = -\mathbf{C}_{\text{FE}} \mathbf{p}, \quad (32)$$

where  $\mathbf{C}_{\text{FE}}$  is assembled of the element matrices

$$\mathbf{C}_{\text{FE}}^k = - \int_{\tau_k} \mathbf{N}_u^T \mathbf{n}^k \mathbf{N}_p \, ds_x. \quad (33)$$

Here, the matrices with the shape functions of the structure and the fluid are denoted by  $\mathbf{N}_u$  and  $\mathbf{N}_p$ , respectively. A lumped force loading is applied, which neglects moments. Please note, that only nodes on the coupling interface  $\Gamma_1$  have non-zero entries in  $\mathbf{C}_{\text{FE}}$ . All other entries, including those resulting from rotational degrees of freedom, are simply set to zero. Piecewise linear and bilinear shape functions are applied for  $\mathbf{N}_p$  and  $\mathbf{N}_u$ .

Due to the second transmission condition (7), the acoustic flux  $q$  on each boundary element  $\tau_m$  is computed from the structural displacements of the adjacent nodes  $k$  by

$$\mathbf{q} = \mathbf{T}_q \mathbf{u}. \quad (34)$$

where each row corresponds to

$$q_m = \frac{1}{3} \rho_f \omega^2 \sum_{k \in m} \mathbf{u}_k \cdot \mathbf{n}^m, \quad (35)$$

with the fluid density  $\rho_f$ . This projection is a simple averaging which turned out to be suitable for engineering applications [39]. Again,  $\mathbf{T}_q$  has zero entries for rotational degrees of freedom and those related to interior structure nodes.

As outlined in [39], substituting  $\mathbf{q}$  in the BE system (15) by (34) and  $\mathbf{f}_f$  in the FE system (30) by (32) and eliminating  $\mathbf{u}$  from the BE system (15) by (30) yields a Schur complement representation of the coupled system

$$\underbrace{(\mathbf{K}_{\text{BE}} - \mathbf{C}_{\text{BE}} \mathbf{T}_q \mathbf{K}_{\text{FE}}^{-1} \mathbf{C}_{\text{FE}})}_{=: \mathbf{S}} \mathbf{p} = -\mathbf{C}_{\text{BE}} \mathbf{T}_q \mathbf{K}_{\text{FE}}^{-1} \mathbf{f}_s, \quad (36)$$

where  $\mathbf{S}$  denotes the Schur complement.

In the following, a GMRES solver is applied for solving (36). A simple diagonal scaling or an incomplete LU factorization of the near-field of  $\mathbf{K}_{\text{BE}}$  is applied as preconditioner. The matrix-vector product with  $\mathbf{K}_{\text{BE}}$  and  $\mathbf{C}_{\text{BE}}$  is evaluated using the fast multipole method. Two near-field matrices are set-up, one for  $\mathbf{K}_{\text{BE}}$  and one for  $\mathbf{C}_{\text{BE}}$ . Please note, only a single multipole cycle is needed per iteration step. The far-field signature has to be computed separately for the two loads. The remaining steps are done simultaneously. Especially, the integration of the far-field contribution in the leaf clusters only has to be recovered once. The inner inverse  $\mathbf{K}_{\text{FE}}^{-1}$  is computed by a  $LDL^T$  factorization.

## 6 Numerical Results

In this section, the proposed coupling approach is applied to the vibro-acoustic simulation of a cylindrical test structure. First, the test scenario is outlined in the following section. Then, the pure BE half-space problem is investigated, using an artificial analytical sound field. After this, the results of a fully coupled simulation are discussed. Finally, the efficiency of the proposed approach is considered.

### 6.1 Test Scenario

The cylindrical test structure is depicted in Figure 4 (a) and (b). The hull consists of a 20 m long cylinder with a radius of 1 m. At both ends, circular disks and hemispherical endcaps are mounted, resulting in a total length of 22 m. The internal structure consists of ring stiffeners, which are inserted every 0.8 m along the center line. In longitudinal direction, stiffeners are located every  $30^\circ$  with respect to the center line. Additionally, the structure is strengthened by an intermediate floor, which is again supported by stiffeners in longitudinal and transverse direction. The thickness of all components is 1.5 cm, and steel (Young's modulus=207 GPa, Poisson's ratio=0.3, density  $\rho_s=7669 \text{ kg/m}^3$ ) is used as material.



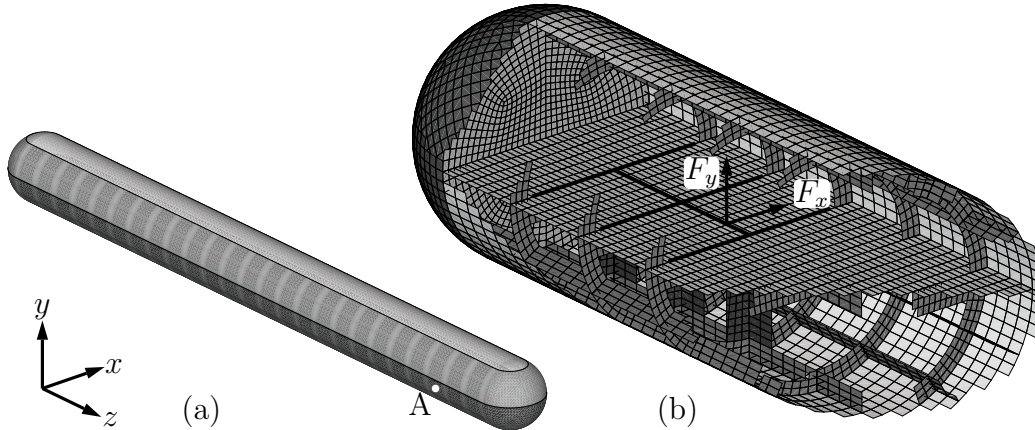


Figure 4: Cylindrical test structure with waterlines (a) and internal structure with driving forces (b).

The test structure is partly immersed in water ( $\rho_f=1000\text{kg/m}^3$ ,  $c_f=1387\text{m/s}$ ). The vibro-acoustic behavior for two different drafts is investigated. In the first case, the waterline is at a distance of 1 m above the bottom of the hull, i.e. exactly one half of the structure is submerged. Thus, the black part in Figure 4 (a) is in contact with the water. The other waterline in the second case is at a height of  $(1+\sin 60^\circ)\text{m} \approx 1.866\text{m}$ . In this case, also the dark gray part of the structure is immersed.

The finite element model consists of 32,812 quadrilateral and 128 triangular elements of the ANSYS type SHELL181. Thus, the number of structural degrees of freedom is 186,774. Rayleigh damping as defined in (31) with  $\alpha_D = 1\text{ s}^{-1}$  and  $\beta_D = 5 \cdot 10^{-6}\text{ s}$  is applied for this model. A conforming coupling scheme is applied. The boundary element mesh for the fluid part is directly generated from the faces of the structure elements. A quadrilateral element is transferred to two triangular boundary elements. The number of fluid degrees of freedom is 6,059 for the 1 m draft and 10,403 for the draft with 1.866 m, respectively.

The structure is excited by 194 forces. These act at all nodes which are marked by the black lines in Figure 4 (b). Only two forces are plotted exemplarily. In this area of the model, additional cross-shaped ribs are integrated below the bottom. The first 97 forces act in  $x$ -direction. The remaining 97 forces act in  $y$ -direction and have a phase shift of  $\pi/2$ . All forces have an artificial amplitude of 1 N. These forces may result from an unbalance due to a combustion engine or auxiliary equipment.

## 6.2 Simulation Error of the Acoustic Problem

In this subsection, only the acoustic part of the problem and its simulation error is considered. The structural domain is neglected completely. An analytic sound field is generated using nine monopole sources, which are uniformly distributed along the center line with a distance of 2.5 m in-between each other. To fulfill the Dirichlet boundary condition on the fluid surface, the monopole sources have to be mirrored on the half-space plane and sup-

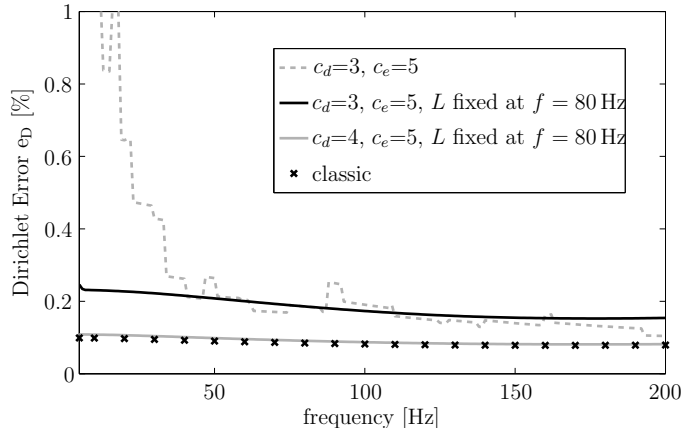


Figure 5: Dirichlet error  $e_D$  of the pure acoustical problem for different multipole parameters.

plied with a negative strength as demanded by (10). The acoustic flux  $q$  is then computed for every boundary element and directly used as boundary condition instead of the transmission condition (7). The multipole BEM is applied to compute the pressure  $\mathbf{p}$  on the nodes. Since the analytical pressure distribution  $\mathbf{p}_{\text{mono}}$  is known by (10), too, the Dirichlet error

$$e_D = \frac{\|\mathbf{p} - \mathbf{p}_{\text{mono}}\|_{L_2}}{\|\mathbf{p}_{\text{mono}}\|_{L_2}} \quad (37)$$

can be computed, where  $\|\cdot\|_{L_2}$  denotes the  $L_2$ -norm. The model with 1.886 m draft is considered in the following. The Dirichlet errors  $e_D$  for the frequency range  $f = [5 \text{ Hz}, 200 \text{ Hz}]$  are visualized in Figure 5 for different expansion lengths. Obviously, the naive use of the semi-empirical rule (20) for the expansion length with  $c_e=5$  results in low errors for the higher frequencies (dashed gray line). But for lower frequencies, the error increases rapidly. The reason for this is the large ratio of elements per wavelength, which is 142 at  $f=100$  Hz. However, the semi-empirical rule (20) is optimized for 6-10 elements per wavelength. This small element size is needed for the structural domain. Since a conforming coupling scheme is used, the same element size also has to be used for the BE part. But if the semi-empirical rule (20) is evaluated at a given frequency  $f = 80$  Hz and the expansion lengths on the different levels are kept fixed for all frequencies, the result looks much better (black line). For engineering applications, an error of approximately 0.2% is often sufficient. Consequently, this parameter set is chosen for all simulations of the coupled problem. If the near-field parameter  $c_d = 4$  is used (gray line), hardly any difference compared to the classical solution without FMM is observable (crosses), which shows the correct implementation of the half-space FMM.

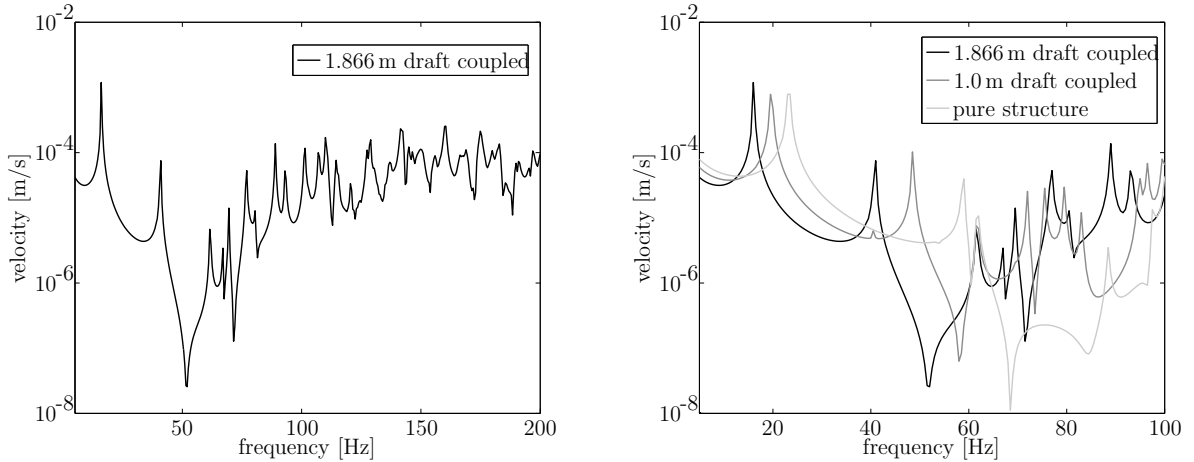


Figure 6: Velocity in  $x$ -direction at node A (see Figure 4) for the frequency range up to 200 Hz (left). Comparison of the velocity response for different drafts (right).

### 6.3 Results of the Coupled Fast BE-FE Simulation

Now, the fully coupled system (36) is investigated. Therefore, a simulation is performed every 0.5 Hz up to 200 Hz. The velocities in  $x$ -direction for node A (cf. Figure 4) are visualized in Figure 6. The first eigenmodes in the low frequency regime correspond to the global beam-like modes. Here, the different modes are clearly separated. Since point A is located on the hull between the nearby stiffeners, also local modes are observed in the higher frequency regime, see Figure 6 (left). Altogether, the velocity range covers five orders of magnitude.

In Figure 6 (right), the frequency response is analyzed for different drafts. Starting from the pure structural response, i.e. without any surrounding water, the resonance frequencies of the global modes decrease with an increasing waterline as expected. This decrease is especially observable for the second mode, which is shifted from 60 Hz for the pure structural problem to 40 Hz in case of the 1.866 m draft. This investigation clearly shows, that a strong coupling scheme is absolutely necessary, since the water has a significant influence on the vibration behavior of the structure.

### 6.4 Efficiency of the Half-Space Fast BEM

In this subsection, the efficiency of the fast multipole implementation of the half-space problem is discussed. First, the number of computed and applied translation operators is investigated. Since a regular clustering is applied, the translation operators can be reused for the same kind of translation on a given level. Thus, the number of computed operators differs from the number of performed translations, as summarized in Table 1. The original model corresponds to the non-mirrored model and reflects the application of the standard multipole implementation as used in [39]. This is physically not meaningful, but it allows to detect the additional expenses, which are necessary for considering the half-space problem.

Table 1: Number of computed and applied translation operators on the different levels  $\ell$ .

level $\ell$	computed			applied		
	original	mirrored	increase %	original	mirrored	increase %
$\hat{\ell} - 12$	–	8	–	–	12	–
$\hat{\ell} - 11$	12	8	–33.3	42	36	–14.2
$\hat{\ell} - 10$	2	4	100.0	14	28	100.0
$\hat{\ell} - 9$	0	0	–	0	0	–
$\hat{\ell} - 8$	8	28	250.0	80	592	640.0
$\hat{\ell} - 7$	48	67	39.6	1264	2228	76.2
$\hat{\ell} - 6$	54	81	50.0	2120	4160	96.2
$\hat{\ell} - 5$	166	184	10.8	6628	8936	34.8
$\hat{\ell} - 4$	230	230	0.0	11914	14162	18.9
$\hat{\ell} - 3$	188	190	1.0	15662	18002	14.9
$\hat{\ell} - 2$	264	264	0.0	15730	18494	17.6
$\hat{\ell} - 1$	286	286	0.0	29168	34642	18.8
$\hat{\ell}$	172	176	2.3	1344	1544	14.9
$\Sigma$	1430	1526	6.7	83966	102836	22.5

Please note, that the mirrored model has one additional cluster-level due to the doubled geometry.

The number of computed translation operators hardly increases for levels with small clusters, being close to the maximum level  $\hat{\ell}$ . Only on the coarser levels one can observe a growth. This reflects the fact, that most of the interaction to the mirrored part takes place on coarser levels due to well separated clusters. This way, the overall number of computed translation operators only increases by 6.7%. Thus, the memory consumption for storing the translation operators remains almost unchanged.

A similar behavior is observed for the applied translations for a single multipole cycle. As before, the number of translations increases only slightly for small clusters and more significantly for the big ones. The overall increase of applied translations is 22.5%, which reflects the fact, that the far-field compression with the multipole expansion helps to efficiently implement the half-space fundamental solution. This increase is directly linked to the additional time, needed for the translations to the mirrored part.

**Remark 1** *A mathematical asymptotical analysis of the amount of translations in the described Fast Multipole Method for the half-space problem shows that the percentage of the additional translations is further reduced for larger numbers of unknowns.*

The computational times for the different operations of the far-field within a single multipole cycle are summarized in Table 2. As before, the original non-mirrored model is compared with the mirrored one. All times are normalized with respect to the total time, needed for a cycle of the original model. The computational times for the far-field signa-

Table 2: Computational times for the far-field portion of the matrix-vector product. The times are normalized with respect to the total time of the original model.

multipole part		original	mirrored	increase %
far-field signature	(26)	71.9	71.7	-0.2
translation	(27)	7.4	9.0	22.6
outer-outer	(28)	2.2	2.2	0.0
inner-inner	(29)	2.1	4.2	100.0
recover	(22)	16.4	32.4	97.6
$\Sigma$		100.0	119.5	19.5

ture (26) and the outer-outer transformation (28) do not change since the source clusters are not mirrored. The slight difference between 71.9 and 71.7 is caused by measurement errors. As pointed out before, the number of applications of the translation operators (27) grows and consequently the computational time increases by 22.6%. In the opposite direction, the inner-inner transformation (29) and the recovery of the solution by (22) has to be performed for the original and the mirrored clusters and therefore takes approximately twice as much time. Focusing on the total computational time for a single cycle, the increase is only 19.5%. This is because most of the time is spent for the computation of the far-field signature and this part remains unmodified.

Besides the far-field, where the multipole expansion is applied, a near-field has to be set-up by standard BEM. As pointed out before, for large models, most of the interaction to the mirrored part is covered by the far-field. For this model, only 7.1% of the total integration time for the mirrored model is spent for the additional mirrored part. If both the near-field and the far-field are taken into consideration, the additional computational time for the multipole implementation of the half-space problem is below 20% with respect to the original model without half-space. In case of a classical implementation, the expense may be up to 100%.

Beside the expense of a single cycle, also the number of needed iteration steps for the GMRES solver is of significant importance. In the following a relative accuracy of  $10^{-6}$  is applied for the solver. The numbers of iteration steps for different drafts and preconditioners are visualized in Figure 7. In the left subfigure, the two different drafts are analyzed using a diagonal scaling as preconditioner. In case of the 1.866 m draft, also the numbers of iteration steps for the one-way coupled case are plotted. One-way coupling means, that  $\mathbf{C}_{\text{FE}}$  of (36) is set to zero and this way the feedback of the pressure is neglected. Since the second part of the Schur complement is neglected for preconditioning, the number of iteration steps is best for the one-way coupled case. Here, one observes only a slight increase for higher frequencies. If a waterline of 1 m is considered and a strong coupling is applied, the number of iteration steps increases with the frequency. For a larger draft this number is even larger.

In Figure 7 (right), the scaling preconditioner is compared to an ILU preconditioner applied to the near-field of  $\mathbf{K}_{\text{BE}}$ . For high frequencies, the numbers of iteration steps are

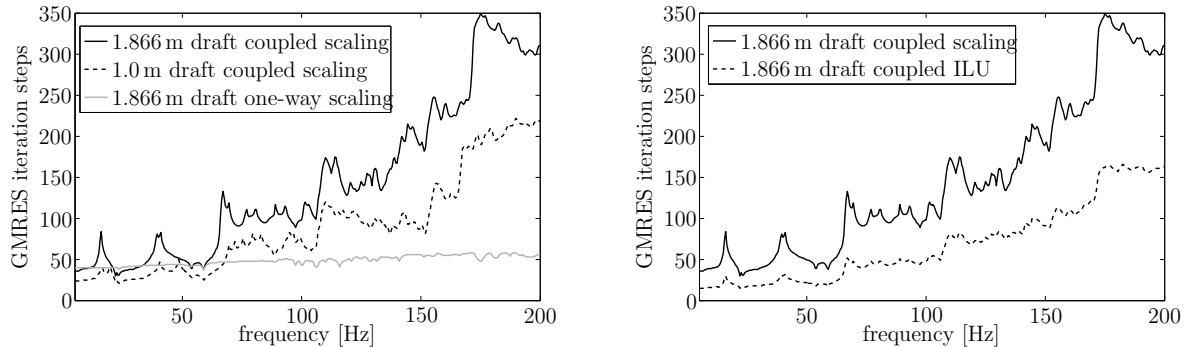


Figure 7: Number of iteration steps with diagonal scaling preconditioner for different drafts (left). Comparison of scaling and ILU preconditioner for 1.866 m draft (right).

significantly reduced. At 200 Hz, a reduction by a factor of 2 is obtained. But this is achieved to the expense of an additional memory consumption, since the near-field has to be stored a second time for the ILU factorization. Concerning this issue, a simple scaling is much cheaper. The used preconditioners neglect the second part of the Schur complement and therefore correspond to the one-way coupling. Since there is a significant difference between the one-way coupled and fully coupled solution, these preconditioners can not be optimal. Further research is needed to develop advanced preconditioners for the coupled system.

## 7 Conclusion

A coupling scheme for fluid-structure interaction using a fast multipole boundary element method and a finite element method is presented. Special focus is on partly immersed bodies, where a free fluid surface exists. A special half-space fundamental solution is applied, which allows to incorporate the Dirichlet boundary condition on the half-space plane. The modifications of the fast multipole method for half-space problems are pointed out. Due to the use of a mirror technique, most of the standard multipole procedures can be applied. Additionally, this results in a good far-field compression of the introduced mirrored part. The numerical efficiency concerning the computational time is examined for a realistic model problem. The additional expense for the incorporation of the half-space surface turns out to be small with respect to the overall expense.

## Acknowledgement

This research was financially supported by the German Research Foundation (DFG) under the transfer project SFB404/T3 conducted jointly between Institute of Applied and Experimental Mechanics at University of Stuttgart and Germanischer Lloyd AG. The authors acknowledge valuable contributions of Dr. Christian Cabos and Marc Wilken of Germanischer Lloyd AG, Hamburg.

## References

- [1] Kinsler LE, Frey AR, Coppens AB, Sanders JV. *Fundamentals of Acoustics*. 4th edn., John Wiley & Sons, Inc., 2000.
- [2] Fahy FJ. *Sound and Structural Vibration: Radiation, Transmission and Response*. Elsevier Press, Amsterdam, Heidelberg, 2007.
- [3] Philippi P, Habault D, Lefebvre JP, Bergassoli A. *Acoustics. Basic Physics, Theory and Methods*. Academic Press, San Diego, 1999.
- [4] Zienkiewicz OC, Taylor RL. *The Finite Element Method, Volume 1: The Basis*. Butterworth Heinemann Oxford, 2000.
- [5] Gaul L, Kögl M, Wagner M. *Boundary Element Methods for Engineers and Scientists. An Introductory Course with Advanced Topics*. Springer Berlin, 2003.
- [6] Nédélec JC. *Acoustic and Electromagnetic Equations: Integral Representations for Harmonic Problems*. Applied Mathematical Sciences 144, Springer New York, 2001.
- [7] Rjasanow S, Steinbach O. *The Fast Solution of Boundary Integral Equations*. Springer New York, 2007.
- [8] Marburg S, Nolte B (eds.). *Computational Acoustics of Noise Propagation in Fluids*. Springer Berlin, 2008.
- [9] Wu TW (ed.). *Boundary Element Acoustics. Fundamentals and Computer Codes*. WIT Press Southampton, 2000.
- [10] Schenk HA. Improved integral formulations for acoustic radiation problems. *J. Acoust. Soc. Am.* 1968; **44(1)**:41–58.
- [11] Brakhage H, Werner P. Über das Dirichletsche Außenraumproblem für die Helmholtzsche schwingungsgleichung. *Archiv der Mathematik* 1965; **16**:325–329.
- [12] Burton AJ, Miller GF. The application of integral equation methods for the numerical solution of boundary value problems. *Proc. Roy. Soc. London A* 1971; **232**:201–210.
- [13] Buffa A, Hiptmair R. Regularized combined field integral equations. *Numer. Math.* 2005; **100(1)**:1–19.
- [14] S. Engleder, O. Steinbach: Stabilized boundary element methods for exterior Helmholtz problems. *Numer. Math.* 2008; **110**: 145–160.
- [15] Saad Y. *Iterative Methods for Sparse Linear Systems*. PWS, 2003.
- [16] Ochmann M, Himm A, Makarov S, Semenov S. An iterative GMRES-based boundary element solver for acoustic scattering. *Eng. Anal. Bound. Elem.* 2003; **27**:714–725.

- [17] Rokhlin V. Rapid solution of integral equations of classical potential theory. *J. Comput. Phys.* 1985; **60**:187–207.
- [18] Rokhlin V. Diagonal forms of translation operators for the Helmholtz equation. *Appl. Comput. Harmon. A.* 1993; **1**:82–93.
- [19] Epton MA, Dembart B. Multipole translation theory for the tree-dimensional Laplace and Helmholtz equation. *SIAM J. Sci. Comput.* 1995; **16**(4):865–897.
- [20] Rahola J. Diagonal forms of the translation operators in the fast multipole algorithm for scattering problems. *BIT* 1996; **36**(2):333–358.
- [21] Amini S, Profit ATJ. Multi-level fast multipole solution of a scattering problem. *Eng. Anal. Bound. Elem.* 2003; **27**:547–564.
- [22] Nishimura N. Fast multipole accelerated boundary integral equation methods. *Appl. Mech. Rev.* 2002; **55**:299–324.
- [23] Gumerov NA, Duraiswami R. *Fast Multipole Methods for the Helmholtz Equation in Three Dimensions*. Elsevier, Oxford, 2004.
- [24] Sakuma T, Yasuda Y. Fast multipole boundary element method for large-scale steady-state sound field analysis, part I: Setup and validation. *Acta Acust. United Ac.* 2002; **88**:513–525.
- [25] Schneider S. Application of fast methods for acoustic scattering and radiation problems. *J. Comput. Acoust.* 2003; **11**:387–401.
- [26] Shen L, Liu YJ. An adaptive fast multipole boundary element method for three-dimensional acoustic wave problems based on the Burton-Miller approach. *Comput. Mech.* 2007; **40**:461–472.
- [27] Fischer M. The fast multipole boundary element method and its application to structure-acoustic field interaction. PhD Thesis, University of Stuttgart 2004.
- [28] Hackbusch W. A sparse matrix arithmetic based on H-matrices I. introduction to H-matrices. *Computing* 1999; **62**(2):89–108.
- [29] Bebendorf M. *Hierarchical Matrices, A Means to Efficiently Solve Elliptic Boundary Value Problems*. Springer Berlin, Heidelberg, 2008.
- [30] Buchau A, Rucker W, Rain O, Rischmüller V, Kurz S, Rjasanow S. Comparison between different approaches for fast and efficient 3-D BEM computations. *IEEE T. Magn.* 2003; **39**:1107–1110.
- [31] Forster H, Schrefl T, Dittrich R, Scholz W, Fidler J. Fast boundary methods for magnetostatic interactions in micromagnetics. *IEEE T. Magn.* 2003; **39**:2513–2515.



- [32] Seybert AF, Soenarko B. Radiation and scattering of acoustic waves from bodies of arbitrary shape in a three-dimensional half space. *Transactions of the ASME* 1988; **110**:112–117.
- [33] Seybert A, Wu T. Modified Helmholtz integral equation for bodies sitting on an infinite plane. *J. Acoust. Soc. Am.* 1989; **85**:19–23.
- [34] Sladek V, Tanaka M, Sladek J. Revised Helmholtz integral equation for bodies sitting on an infinite plane. *Trans. of JSCEs* 2001; **3**:35–40.
- [35] Junger MC, Feit D. *Sound, Structures, and Their Interaction: Basic Concepts*. 2nd edn., The MIT Press, 1986.
- [36] Wilton DT. Acoustic radiation and scattering from elastic structures. *Int. J. Numer. Meth. Eng.* 1978; **13**:123–138.
- [37] Amini S, Harris PJ, Wilton DT. *Coupled Boundary and Finite Element Methods for the Solution of the Dynamic Fluid-Structure Interaction Problem*. Springer Berlin, 1992.
- [38] Hughes MD, Chen K. An efficient preconditioned iterative solver for solving a coupled fluid structure interaction problem. *International Journal for Computer Mathematics* 2004; **81**:583–594.
- [39] Brunner D, Junge M, Gaul L. A comparison of FE-BE coupling schemes for large scale problems with fluid-structure interaction. *Int. J. Numer. Meth. Eng.* 2008; **in press**, DOI: [10.1002/nme.2412](https://doi.org/10.1002/nme.2412).
- [40] Brunner D, Junge M, Cabos C, Gaul L. Vibroacoustic simulation of partly immersed bodies by a coupled fast BE-FE approach. *Proceedings of EuroNoise '08, Paris, CDROM*. 2008.
- [41] Brunner D, Junge M, Wilken M, Cabos C, Gaul L. Vibro-acoustic simulations of ships by coupled fast BE-FE approaches. *Proceedings of IMAC XXVII: Conference & Exposition on Structural Dynamics, Orlando, CDROM*. 2009.
- [42] Gyure MF, Stalzer MA. A prescription for the multilevel Helmholtz FMM. *IEEE Comput. Sci. Eng.* 1998; **5**:39–47.
- [43] Bathe KJ. *Finite Element Procedures*. Prentice-Hall, Englewood Cliffs, 1995.
- [44] Ansys. *Guide for Interfacing with Ansys: Release 10.0* 2005.

## Erschienene Preprints ab Nummer 2006/1

- 2006/1 S. Engleder, O. Steinbach: Modified Boundary Integral Formulations for the Helmholtz Equation.
- 2006/2 O. Steinbach (ed.): 2nd Austrian Numerical Analysis Day. Book of Abstracts.
- 2006/3 B. Muth, G. Of, P. Eberhard, O. Steinbach: Collision Detection for Complicated Polyhedra Using the Fast Multipole Method of Ray Crossing.
- 2006/4 G. Of, B. Schneider: Numerical Tests for the Recovery of the Gravity Field by Fast Boundary Element Methods.
- 2006/5 U. Langer, O. Steinbach, W. L. Wendland (eds.): 4th Workshop on Fast Boundary Element Methods in Industrial Applications. Book of Abstracts.
- 2006/6 O. Steinbach (ed.): Jahresbericht 2005/2006.
- 2006/7 G. Of: The All-floating BETI Method: Numerical Results.
- 2006/8 P. Urthaler, G. Of, O. Steinbach: Automatische Positionierung von FEM-Netzen.
- 2006/9 O. Steinbach: Challenges and Applications of Boundary Element Domain Decomposition Methods.
- 2006/10 S. Engleder: Stabilisierte Randintegralgleichungen für äussere Randwertprobleme der Helmholtz-Gleichung.
- 2007/1 M. Windisch: Modifizierte Randintegralgleichungen für elektromagnetische Streuprobleme.
- 2007/2 M. Kaltenbacher, G. Of, O. Steinbach: Fast Multipole Boundary Element Method for Electrostatic Field Computations.
- 2007/3 G. Of, A. Schwaigkofler, O. Steinbach: Boundary integral equation methods for inverse problems in electrical engineering.
- 2007/4 S. Engleder, O. Steinbach: Stabilized Boundary Element Methods for Exterior Helmholtz Problems.
- 2007/5 O. Steinbach, G. Unger: A Boundary Element Method for the Dirichlet Eigenvalue Problem of the Laplace Operator.
- 2007/6 O. Steinbach, M. Windisch: Modified combined field integral equations for electromagnetic scattering.
- 2007/7 S. Gemmrich, N. Nigam, O. Steinbach: Boundary Integral Equations for the Laplace-Beltrami Operator.
- 2007/8 G. Of: An efficient algebraic multigrid preconditioner for a fast multipole boundary element method.
- 2007/9 O. Steinbach (ed.): Jahresbericht 2006/2007.
- 2007/10 U. Langer, O. Steinbach, W. L. Wendland (eds.): 5th Workshop on Fast Boundary Element Methods in Industrial Applications, Book of Abstracts
- 2008/1 P. Urthaler: Schnelle Auswertung von Volumenpotentialen in der Randelementmethode
- 2008/2 O. Steinbach (ed.): Workshop on Numerical Simulation of the Maxwell Equations. Book of Abstracts.
- 2008/3 G. Of, O. Steinbach, P. Urthaler: Fast Evaluation of Newton Potentials in the Boundary Element Method.
- 2008/4 U. Langer, O. Steinbach, W. L. Wendland (eds.): 6th Workshop on Fast Boundary Element Methods in Industrial Applications, Book of Abstracts